

Nanotechnology Research and Development for Military and Industrial Applications

Paul B. Ruffin^a, Christina L. Brantley^a, Eugene Edwards^a, J. Keith Roberts^a, William Chew^a, Larry C. Warren^a, Paul R. Ashley^a, Henry O. Everitt^a, Eric Webster^a, John V. Foreman^a, Mohan Sanghadasa^a, Sihon H. Crutcher^a, Mark G. Temmen^a, Vijay Varadan^b, Devlin Hayduke^c, Pae C. Wu^d, Christopher G. Khoury^d, Yang Yang^d, Tong-Ho Kim^d, Tuan Vo-Dinh^d, April S. Brown^d, John Callahan^e

^aU. S. Army Research, Development, and Engineering Command
Redstone Arsenal, Alabama 35898
E-mail: paul.ruffin@us.army.mil
Phone: 256-876-8333

^bUniversity of Arkansas, Fayetteville, Arkansas 72701

^cMaterial Sciences Corporation, 135 Rock Road, Horsham, Pennsylvania 19044

^dDuke University, Durham, North Carolina 27708

^eAEgis Technologies Group, Inc, 631 Discovery Dr. NW, Huntsville, Alabama 35806

ABSTRACT

Researchers at the Army Aviation and Missile Research, Development, and Engineering Center (AMRDEC) have initiated multidiscipline efforts to develop nano-based structures and components for insertion into advanced missile, aviation, and autonomous air and ground systems. The objective of the research is to exploit unique phenomena for the development of novel technology to enhance warfighter capabilities and produce precision weapons. The key technology areas that the authors are exploring include nano-based microsensors, nano-energetics, nano-batteries, nano-composites, and nano-plasmonics. By integrating nano-based devices, structures, and materials into weaponry, the Army can revolutionize existing (and future) missile systems by significantly reducing the size, weight and cost. The major research thrust areas include the development of chemical sensors to detect rocket motor off-gassing and toxic industrial chemicals; the development of highly sensitive/selective, self-powered miniaturized acoustic sensors for battlefield surveillance and reconnaissance; the development of a minimum signature solid propellant with increased ballistic and physical properties that meet insensitive munitions requirements; the development of nano-structured material for higher voltage thermal batteries and higher energy density storage; the development of advanced composite materials that provide high frequency damping for inertial measurement units' packaging; and the development of metallic nanostructures for ultraviolet surface enhanced Raman spectroscopy. The current status of the overall AMRDEC Nanotechnology research efforts is disclosed in this paper. Critical technical challenges, for the various technologies, are presented. The authors' approach for overcoming technical barriers and achieving required performance is also discussed. Finally, the roadmap for each technology, as well as the overall program, is presented.

Keywords: nano-based microsensors, nanotechnology, nano-energetics, nano-composites, and nano-plasmonics

1. INTRODUCTION

There is a need and urgency for the capability to detect/ monitor missile out-gassing, reduce heat generated by sensor / guidance electronics, and reduce the health hazards of solid/ gel propellants in the Army's missile systems. Missile propellants emit gasses that are harmful to humans, can damage sensitive missile components, and can potentially cause deterioration to the missile structure. Nanosensors offer a solution to cost, size, and weight issues associated with smart networked sensor systems designed for missile health monitoring and rocket out-gassing/fuel leak detection.¹ The use of

nanocomposites for missile structures will provide a method to reduce missile weight, electronics overheating, and structural damage. Nanoenergetic based propellants offer a solution to a safer and more environmentally friendly missile propellant. By combining these critical areas of research, a smaller, lighter, cheaper and safer missile/munition can be developed to satisfy current and future mission requirements.

The Applied Nanotechnology for Aviation and Missile Components/Systems program objective is to develop nano structures/components, nanosensors, nanoparticles for energetics, and nanoelectronics/Nanoelectromechanical System (NEMS) for insertion in missile, aviation, and unmanned aerial vehicles (UAV)/unmanned ground vehicles (UGV) systems. The primary objective of the program is to advance the specific candidate nano technologies for successful demonstration of application requirements by basic and applied research. The program, although exploring a wide variety of nanotechnology areas, is currently focused in four key technology areas, 1) Nanosensors, 2) NanoComposites, 3) Nanoenergetics, and 4) Nanoplasmonics; associated miniature electronics are likewise included. The technical issues being addressed are materials development, molecular interactions, quantum effects, and process technology.

In this paper, the AMRDEC research team's current program status, accomplishments, and technical challenges are presented for each of the technology areas. The advanced nano-based microsensors designs, tests, and technical challenges are addressed in Section 2. Multiple methodologies for chemical and acoustic sensing are described, including nanowires, voltammetry, microfluidics, nanofluidics, and Raman based sensing systems. Section 3, addresses the second thrust area associated with NanoEnergetics. The third thrust area, NanoComposites, is presented in Section 4; the development of nano-composite structures to provide enhanced vibratory protection, for the weaponry's Inertial Measurement Unit, is likewise described. Section 5, regarding NanoPlasmonics, addresses the implementation of enhanced chemical detector efficiency via the development of metallic nanostructures for ultraviolet surface enhanced Raman spectroscopy. The final section of the paper provides the summary, including program developments and future efforts.

2. NANO-BASED MICROSENSORS

2.1 Chemical sensing techniques

The first significant thrust area is the development of advanced technology for the fabrication of an array of chemical sensors for Weaponry Health Monitoring (WHM). The resulting WHM chemical sensors will permit the detection of rocket motor off-gassing (to predict propellant degradation) and more or less eliminate the current need for destructive evaluation of rocket motors. The chemical sensors can also be used for the detection of toxic chemicals. The ideal sensing system is a miniaturized chemical sensor array that can be primarily mounted onto a rocket motor to detect and identify multiple analytes that are associated with propellant off-gassing. The sensor must be ruggedized for military environments and miniaturized for minimal payload additions on rocket motors. It should likewise add insignificant weight when mounted on manned and/or unmanned system for the detection of residue from explosive material. The size, power consumption, and surface temperature dependence of the sensor must be minimized by designing the sensor system in the smallest possible configuration while requiring extremely low power input.²

Design schemes for three different nanotechnology-based materials/techniques (for miniature chemical detection devices or micro sensors) are presented. Chemical sensing systems are constructed using 1) functionalized nanowires integrated with a wireless module, 2) microfluidic nano-enhanced Raman systems, and 3) Self Assembled Monolayer (SAM) nanofluidic systems. The fidelity of each technique is assessed by setting up demonstration models in the laboratory and acquiring experimental data.

2.1.1 Functionalized nanowires

Researchers from AMDREC, in collaborations with Professor V. K. Varadan (University of Arkansas), are developing a wireless system for detecting/monitoring chemical analytes.³ The chemical sensor portion of this technology (with resistance/ohmic output) is capable of detecting and identifying bio-terrorism agents and hazardous gases. The sensing techniques utilize tin oxide (SnO) coated nanowires as the sensing material of the sensor. Vertically aligned gold (Au) nanowires are grown uniformly on the enhanced substrate. When the selectively grown nanowires reach the desired length and density, the sample is prepared from the deposition of the spin coated tin oxide. The coating is achieved using a sol-gel technique in optimum conditions, preparing the SnO coated nanowires for device level fabrication.

2.1.1.1 Design approach

The focus of the design approach is the development of vertically aligned nanostructures and the integration of nanosensors within wireless sensor networks. Device fabrication utilizes low temperature processes to facilitate the nanostructured tin oxide thin film on a silicon substrate. The conductance of the thin film is dependent on the concentration of those gases which can potentially act as reducing agents for any adsorbed oxygen on the surface. Based on this design, the sensor is capable of detecting isopropyl alcohol, ethanol, water vapor, Carbon Monoxide (CO), methane and other gases. The schematic configuration allowing the most acceptable sensitivity and response to chemical analytes is shown in figure 1(a). Figure 1(b) depicts the fabricated devices in comparison to the size of a penny.³

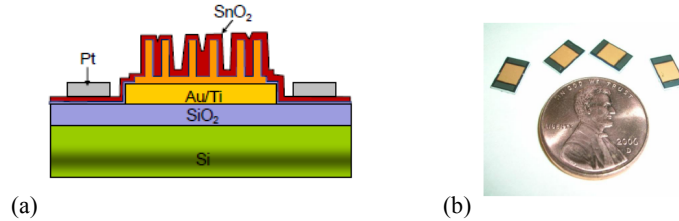


Figure 1. Nanowire Sensor: design concept schematic (a), image of the fabricated devices (b)

The nanosensors are integrated into a wireless system. The wireless system consists of the wireless module and data acquisition board as shown in figure 2. The operation of the wireless gas sensing system is initiated by the resistance change of the nanowire sensor resulting from the change of gas concentration. Afterwards, the pre-amplifier converts resistances to voltage levels and amplifies the signals for conversion to a digital signal interpreted by Analog to Digital Converters (ADC) on the sensor node. The digitized signals are transmitted to the base station (laptop) through wireless transmission. Finally, the base station receives the signals and displays the data on the laptop monitor.³

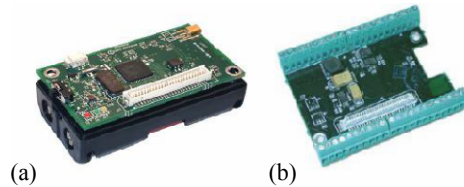


Figure 2. Image of the wireless sensing system: wireless module (a), data acquisition board (b)

2.1.1.2 Experimental results

The resistance changes are amplified via the signal processing and conditioning circuitry and sent wirelessly using a MICA2 wireless module. The data is recorded on a laptop, which is connected to another wireless node acting as a receiver. Figure 3 shows a set of data which has been transformed from raw voltage data to the resistance value of the tin oxide thin-film sensor. The graph clearly depicts the relationship of the sensor resistance to the concentration of Isopropyl Alcohol (IPA).³

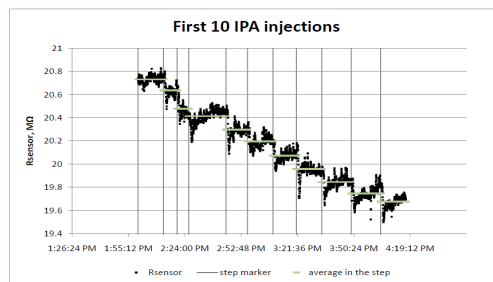


Figure 3. Full data collection run recorded with a tin oxide sensor and the wireless system

The next generation of the nanowire wireless sensing system will combine humidity and temperature sensing with a low power consumption wireless system. Possible refinements to the sensor material include elimination of the heating source, and integration of multiple sensors into a chemical sensor with microelectromechanical systems (MEMS) technology. A lab-on-a-chip, which has onboard data processing and potentially wireless communication capabilities, is ideal for deployment across a wide spectrum of hardware platforms for environmental monitoring and other portable handheld devices.

2.1.1.3 Technical challenges

Designing a nanoscale sensor for chemical detection utilizing functionalized nanowires has significant technical challenges. Controlling the growth of nanowires is very complex, from quantity to quality. Retrieving real-time signal from nanoscale devices has created a challenge due to the requirement for extensive control and characterization of individual sensory elements. Another design hurdle to overcome is the low yield of nanowire assembly in liquid and high contact resistance between electrodes and nanowires. Due to the limited availability of implemented nano-sized electronics for wireless applications, the design of a wireless nanotech sensor has also been difficult.²

2.1.2 Microfluidic nano-enhanced Raman systems

Current research of microfluidic systems include the integration of surface enhanced Raman spectroscopy (SERS) into microfluidic channels^{4,5,6,7}. For instance, Tong and Banerjee research focuses on two dimensional (2D) SERS enhancement, which is limited by a low density of active SERS regions, or hot-spots.^{4,5} Choi's research increased hot-spot density, but does not provide continuous or repeatable flow of material.⁶ In addition, this technique has no control for nanoparticle placement in the analysis chambers. The most promising research of the microfluidic integration of SERS is presented by Goddard.⁷ Goddard's approach includes the tagging of the target molecule with metal nanoparticles and then utilizes laminar microfluidic flow to focus the tagged molecules through a thin analysis region. The Goddard approach is a potential solution, but has limitations to 10 $\mu\text{L}/\text{min}$ flow rates (ideal for DNA detection).

2.1.2.1 Design approach

In collaboration with EngeniusMicro, AMRDEC is developing a microfluidic nano-enhanced Raman system.⁸ The design approach is to develop microfluidic devices capable of preparing and delivering analyte to Surface-Enhanced Raman Spectroscopy (SERS) systems. These devices filter the analyte and shape the flow channel to reduce fluorescence from the bulk fluid. By confining the fluid in a microfluidic device, continuous monitoring, detection of volatile chemicals, and the detection of "stealth" chemicals (not normally detected by Raman Spectroscopy) is possible. The challenge with SERS integration is to embed the modified surface into the microfluidic system and maintain high signal enhancement. The AMRDEC technique utilizes nano-porous membrane SERS chips integrated within microfluidic chips to mitigate signal loss, as well as material and process integration limitations.

2.1.2.2 Experimental results

In order to characterize the SERS response in microfluidic chips with flowing analytes and multiple interfaces, the signal-to-noise ratio of the Raman spectra of liquid rhodamine (with and without a pyrex cover) is evaluated.⁸ Figure 4 shows a 15% reduction in signal-to-noise ratio by applying an optical cover glass to the system. In the experiment, the Raman spectra of liquid rhodamine 6G (R6G) is measured with and without the pyrex optical glass cover. The Raman spectra of the optical dye without the cover is the signal with the highest intensity. The Raman spectra of the signal measured with the optical cover (second signal) results in a 45 to 57% reduction in total spectrum amplitude for an integration time of 1 second. This signal primarily consists of the background fluorescence of rhodamine, and the signal count greater than the fluorescence is shown on the right hand side of the graph. The signal level over the fluorescence amplitude, i.e., signal-to-noise ratio, increases 15% when adding the fluid and Pyrex slide. Another observation of figure 4 is that the quality and accuracy of the Raman spectra of the optical dye is not affected by the pyrex cover. The defining peaks are observed through the pyrex cover.

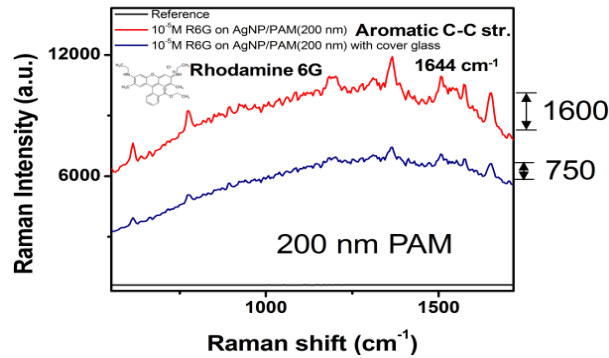


Figure 4. Raman response with and without pyrex cover for Rhodamine6G.

Experimentation, characterizing the effect of interfaces and materials on the SERS response in microfluidic chips, was accomplished when SERS chips were embedded on reflective and non-reflective microfluidic substrates. As shown in figure 5, the Raman spectra of R6G on SERS substrates is measured on a reflective surface (signal with highest intensity) and on a non-reflective surface (signal with lower intensity). The results show that the Raman spectrum of the analyte is not dependent on the underlying surface of the SERS substrate. The defining peaks of R6G are observed on the reflective and non-reflective surfaces.

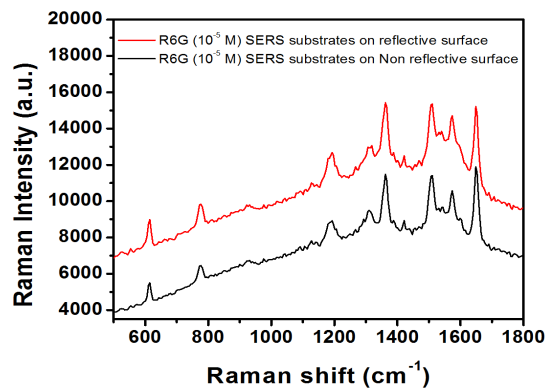


Figure 5. Raman response with and without pyrex cover for Rhodamine6G

Finally, SERS compatibility with silicon-pyrex anodic bonding is investigated, as shown in Figure 6. Figure 6 presents the comparison of Raman spectra from the R6G solution (10^{-5} M) on silver nanoparticles grown inside the Porous Alumina Membrane (PAM) to the spectra for the R6G solution on the same substrate exposed for 30 minutes at $400\text{ }^{\circ}\text{C}$ (anodic bonding occurs). The results demonstrate the potential affect of anodic bonding on the SERS enhancement. The PAM after anodic bonding showed almost no Raman enhancement compared to the PAM before anodic bonding. This indicates that the bonding process might cause the silver nanoparticles to oxidize, leading to reduced SERS enhancement.

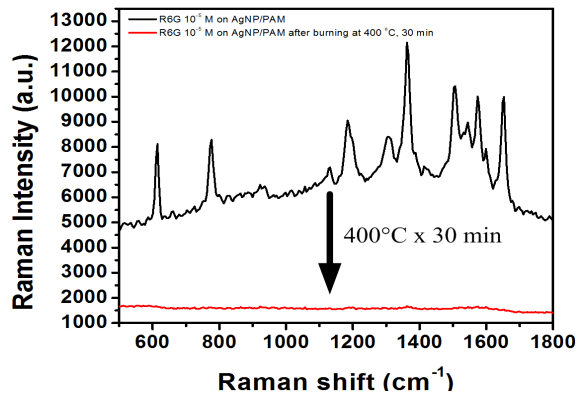


Figure 6. Silver NP based SERS are not compatible with anodic bonding in the presence of oxygen gas

2.1.2.3 Technical challenges

Technical challenges for the development of microfluidic nano-enhanced Raman systems include the need to enhance the signal quality for embedded SERS. Currently, pyrex viewports and silicon wafers show only modest decreases in signal quality for embedded SERS. Possible solutions to optimizing the signal quality include shaping the flow channel to reduce background fluorescence from bulk analyte. In addition, the optical laser can boil the analyte carrier (typically water) causing additional optical scattering; therefore, flow rates should be maintained to limit the fluid temperature.

Another technical challenge is the need to advance microfabrication processes capable of securely embedding the SERS chips. Anodic bonding, for example, is compatible with gold nanoparticles but is not compatible with silver nanoparticles and polymers (due to oxidation). Reliable, low-temperature “stamp-and-stick” or polymer bonding process are promising alternatives for embedded SERS.

2.1.3 Nanofluidic sensors

Novel nanofluidic technology and nanofluidic phenomena, not possible in microfluidic/capillary systems, are used to develop state-of-the-art nanosensor systems for ultra-sensitive detection of biological agents. The system uses the phenomena of charge exclusion based separation and sample preconcentration. The two nanofluidic components for sample preparation include a nano-separator and a nano-preconcentrator. An impedance based electrochemical sensor is integrated with the nanofluidic components to form a handheld biological threat agent detector.⁹

2.1.3.1 Design approach

Scientists from AMRDEC and the Defense Advanced Research Projects Agency (DARPA) have partnered with CFD Research Corporation to investigate different technical approaches to improving chemical detection using recent advances in nanotechnology.⁹

The CFD approach to chemical detection utilizes an impedance-based sensor with gold interdigitated fingers. The electrodes of the sensor are functionalized with Self Assembled Monolayers (SAM). Various categories of these SAMs are highly sensitive to and specific for different chemical compounds. Each functionalized set of electrodes are incorporated as an element into an array of differently functionalized electrodes; each are targeted for different analytes. These detection arrays would then be incorporated into micro or nanofluidic flow cells.

As the solution containing the analytes of interest is introduced into a microfluidic or nanofluidic environment (see Figure 7), a pair of electrodes is energized with an AC field. The induced current is related to the applied voltage and impedance of the system; all of the resulting parameters are in turn dependent on the presence or absence of targeted analytes. The concentrations of analytes and electrolytes impact the impedance in two ways: 1) resistivity of the solution

is a function of its electrical conductivity which depends on the electrolyte and analyte concentrations; and 2) electric double layer (EDL) capacitance is a function of double layer thickness (which in turn is a function of electrolyte concentration) and surface charges at the electrode. Therefore, when a sample with different ionic compositions is flowed through the system, it changes both the EDL capacitance and the solution resistance. The changes are reflected in the form of a change in the induced base current.

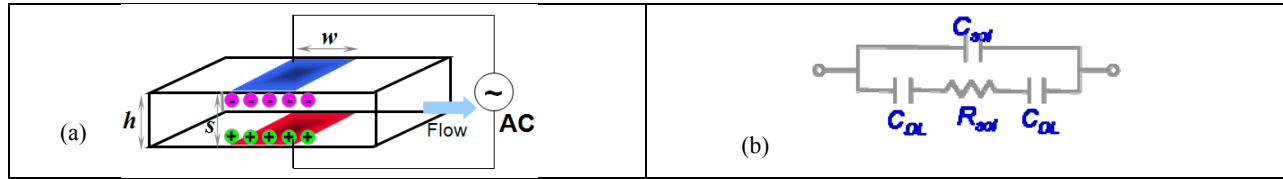


Figure 7. Principle of micro- & nano-impedance-based chemical sensors. (a) microstrip design, (b) the equivalent circuit model

2.1.3.2 Experimental results

During the development and characterization of the electrodes, impedance measurements are made using varying concentrations of ammonia (NH_3). The following concentrations of NH_3 are used: 0.1 mM, 1.0 mM, and 10.0 mM in a 0.2 mM KCl electrolyte solution. The experiments are carried out for various electrode gaps (3, 5 and 7 μm). The results [refer to Figure 8(a)] show a decrease in total impedance with an increase in ammonia concentration. The experimental results also indicate an increase in overall impedance with increasing gap size between electrodes. Figure 8 (b) depicts the total impedance versus the frequency at 7 μm gap size.

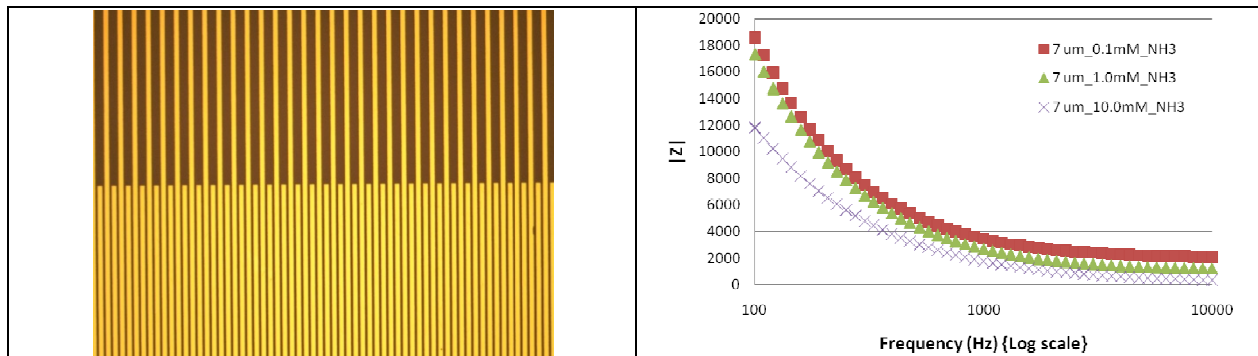


Figure 8. a) 7 μm Gap Electrodes. b) Total Impedance vs. Frequency for the 7 μm Gap Electrodes.

Utilizing flow chambers (obtained from Grace Bio Labs), the static impedance measurements are repeated for varying flow conditions, with flow rates ranging from 0.1 to 10 $\mu\text{L}/\text{min}$. The flow chambers are affixed on top of the impedance chips and flow-induced differential impedance measurements are acquired using a bias voltage of 5 mV and frequencies ranging from 100 to 1000 Hz. The results indicate that for microgap electrodes, the change in impedance in the presence of ammonia is relatively independent of the flow rate.

Future efforts include the investigation of methods to enhance the sensitivity and selectivity of the nano-impedance sensor obtained by SAM modification on the sensor elements (either the gold electrode surface or the inter-electrode glass surface). Additional static impedance testing on sub-micron gap (600, 800 and 1000 nm) electrodes is also planned.

2.2 Acoustic nanosensors

The AMRDEC team is developing ultra miniaturized autonomous piezo-electric acoustic sensors for effective battlefield surveillance & reconnaissance. The primary functions of the sensors are to detect, identify, localize, and track artilleries, aircrafts, vehicles and troop movements. In addition to having tactical advantages in the battlefield, the miniaturization of the acoustic sensors permits the formation of high dense acoustic arrays and hence, allows enhancement in the spatial resolution and bandwidth. However, the frequencies of interest in the battlefield environment are about 0.1 Hz; thereby, imposing a major constraint on the sensor miniaturization. In an attempt to overcome this barrier, AMRDEC's approach is to utilize nanostructured piezo-electric materials for acoustic sensing. This material has the potential to drastically reduce the sensor's size, while maintaining the desired minimum detectable signal (MDS) at the frequencies of interest. A similar technology, based on the broadband electromechanical coupling of piezo-electric nanostructures, is also being considered for scavenging energy from the environment to power auxiliary components (such as wireless communication modules suitable for integration with miniature sensors).

2.2.1 Design approach

In the first phase of this development (Generation 1), the design of the devices was based on a thin annular shaped piezo-electric thin film supported on a thin silicon diaphragm (as illustrated in figure 9). In order to understand the scaling effects of the acoustic sensor, a series of sensors with a wide range of geometries ($D_1 = 190\text{-}760\ \mu\text{m}$ and $D_2 = 250\text{-}1000\ \mu\text{m}$) were designed and fabricated. The sensors represent the smallest piezo-electric acoustic sensors fabricated-to-date¹⁰. The sensors were fabricated on standard 4" silicon-on-insulator (SOI) wafer with 280 nm of silicon on the top and 380 nm of a buried oxide (BOX). Sputter deposited platinum served as the bottom electrode on which 200 nm thick layer of lead zirconate titanate (PZT) solgel was deposited. An e-beam deposited patterned chrome/gold served as the top electrode. A detailed description of the fabrication process has been reported.^{11, 12} An optical micrograph of a fabricated acoustic sensor is shown in figure 9(c).

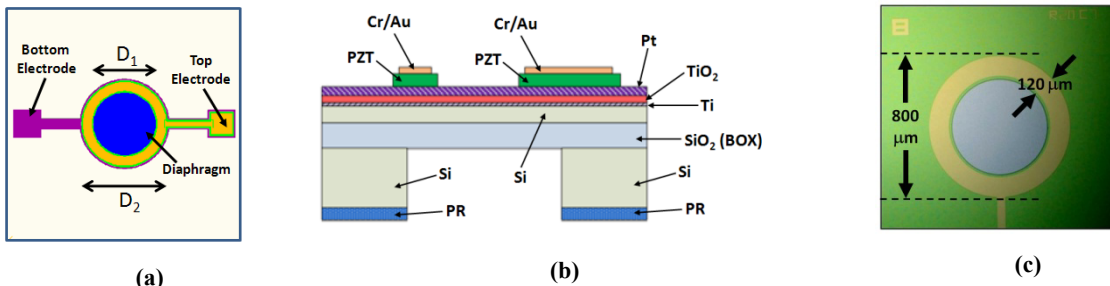


Figure 9. (a) The top view of the acoustic sensor showing the top and bottom electrodes and the diaphragm. (b) A cross-section of the sensor showing layer stack and the etched areas. (c) An optical micrograph of a fabricated acoustic sensor

In order to improve the performance while further miniaturizing the devices, Generation 2 devices were designed using polymer matrix piezoelectric nanocomposites by combining the piezoelectric nanorods in a flexible polymer matrix membrane (see figure 10). Zinc oxide nanorods are used in the current design. Nano structures of new materials with enhanced piezoelectric properties are being considered for the next phase. The intent is to exploit the best properties of both materials. Piezoelectric nanorods provides high electromechanical piezoelectric coupling while the polymer matrix produces a highly compliant, large aspect ratio, ultrathin diaphragm, with low residual stress. Multidimensional scaling (MDS) of a range of devices currently under fabrication has been predicted using a lumped-element analytical model. The size of the devices considered for this modeling varied from a radius of 30 micrometers up to 125 micrometers. The predicted MDS values are shown in [figure 9(b)], along with the data of the Generation 1 devices.

Piezoelectric nanocomposites have also been used in designing miniaturized energy harvesters to power the auxiliary components in the acoustic sensors. Composite materials can be designed to have a low modulus and thus a low resonant frequency. Hence, vibrations can more efficiently be converted to the deformation of the material for mechanical-to-electrical energy conversion in real environments where the vibration spectrum is at far lower frequencies. Furthermore, the high damage threshold of these materials is also an advantage in using them for energy harvesting. Electrospun nano wires/ piezoelectric polymer (PVDF) microfiber and vertically aligned nanowires (embedded in a PVDF for increased

isotropic response or criss-cross for anisotropic response) are used in the current design. Nanowire orientation can be controlled by growth conditions, such as substrate selection, catalyst deposition, temp, gas flow rates, etc. Figure 10(c) shows an SEM image of vertically aligned ZnO nanowires grown on a sapphire substrate.

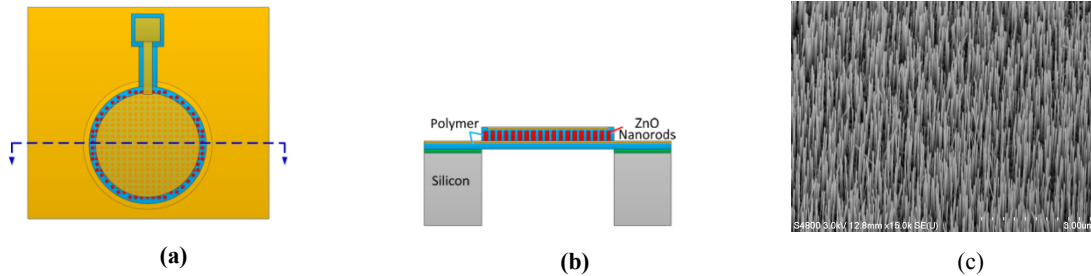


Figure 10. (a) Top-view and (b) cross-section view of the acoustic sensors designed with polymer matrix piezoelectric nanocomposites. (c) SEM images of vertically aligned ZnO nanowires grown on a sapphire substrate.

2.2.2 Experimental results

An acoustic plane wave tube and an anechoic Faraday cage were custom-built for characterizing the sensors for sensitivity, linearity, frequency response and MDS in an environment shielded against exterior acoustic noise and electromagnetic interferences (see figure 11). The tube was designed to limit the propagation of acoustic waves to the fundamental planar mode at frequencies up to 16.88 kHz.

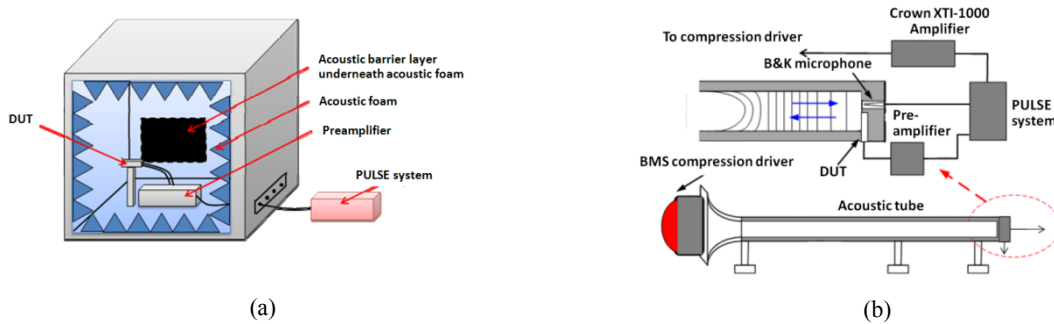


Figure 11. Schematics of (a) the acoustic plane wave tube and (b) the anechoic Faraday cage.

Voltage induced hysteresis loops of all the devices were obtained [figure 12(a)]. The concentric loops shown are as a result of the application of successively increasing the voltage cycling. The hysteresis loops indicated that the polarization that remained after returning from the positive maximum voltage to zero had reached a maximum of $161 \mu\text{C cm}^{-2}$. The sensitivity and the output voltage noise were also measured and hence, the MDS was determined. The sensitivity measured were significantly below predictions, possibly due in part to a reduced piezoelectric coefficient and in part to an increased mechanical stiffness resulting from high residual stress. Despite these differences, the measured sensitivity, noise floor and MDS demonstrated scaling behavior that was consistent with expectations. MDS ranged from below 60 dB SPL for some of the largest devices, up to and over 100 dB SPL for the smallest devices, whereas theory predicted values ranging from 0 dB SPL to 40 dB SPL. The measured MDS values of the devices with data from previously published acoustic sensors¹³⁻¹⁸ are compared in [figure 12(b)].

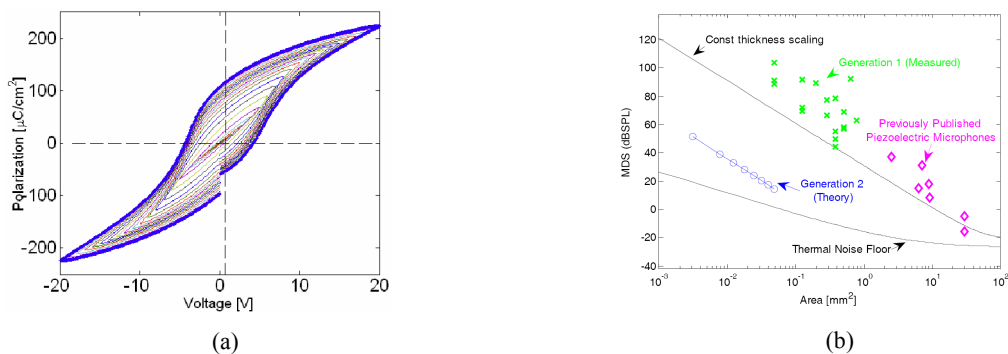


Figure 12. (a) Measured hysteresis loops of polarization versus applied voltage. (b) The measured MDS data of the Generation 1 sensors and the predicted values of the Generation 2 sensors as compared to previously published piezoelectric acoustic sensors reported in the literature¹³⁻¹⁸.

3. NANO- ENERGETICS

The second thrust area is the development of a minimum signature solid propellant with increased ballistic and physical properties that meet Insensitive Munition (IM) requirements. Solid propellants doped with carbon nanotubes (CNTs) could potentially meet the Army's IM requirement. Both multi-walled and single-walled CNTs could perform like rebar when added to a propellant formulation. There is also the potential to increase the burning rate of the propellant by conducting heat below the burning surface of the propellant grain. These are two important and potentially beneficial reasons to evaluate CNTs in propellant formulations. Increasing the burning rate of minimum signature propellants is of great interest to the propellant industry. A doubling of the burning rate of minimum signature propellants has long been the goal. The CNTs are also available with either the hydroxyl (-OH) or carboxyl (-COOH) functional group attached to the carbon structure. The propellant mechanical properties are further enhanced by the addition of the -OH or -COOH functional group, and the bonding of the CNTs to the propellant binder network. The polymer binder network of double-base propellants is primarily formed via hydrogen bonding occurring during the plasticization of nitrocellulose with nitrate-esters. The most common nitrate-esters used in double-base propellants are nitroglycerin (NG) and butanetriol-trinitrate (BTTN). Figure 13 is an SEM image of the structure of the CNTs.

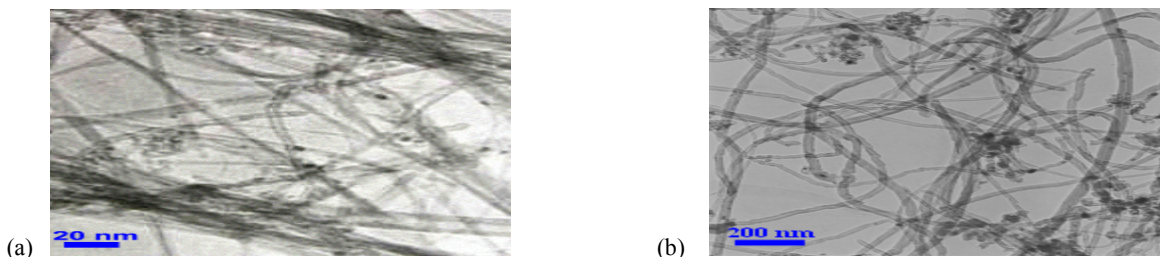


Figure 13. SEMs showing the structure of CNTs, multi-walled (a) and single-walled (b).

3.1 Design approach

The AMRDEC team is currently exploiting the properties of CNTs to improve the physical and performance properties of a potential castable double-base minimum signature propellant formulation. Castable double-base propellant technology is being evaluated extensively in a Joint Insensitive Munitions Technology Program (JIMTP) for potential next generation tactical missile applications with an emphasis on achieving insensitive munitions objectives^{19,20}. The general double-base propellant formulation is a combination of nano particle carbon powders, bismuth and aluminum compounds utilized to control burning rate and burning rate stability. The CNTs were substituted for the carbon powder and the properties of the propellants were compared. Propellant burning rate and rate exponent were determined. A burning rate of at least one inch per second at 1000psi for minimum signature propellants is greatly desired by the military. Achieving the performance objectives and meeting the insensitive munitions requirement is a technical challenge.

In addition to evaluating the burning rate properties of CNTs, the propellant physical properties were assessed. The potential to enhance propellant physical properties (such as stress, strain, modulus, and crosslink density) is an added benefit of the –OH or –COOH functional group attached to the carbon structure of the CNTs.

3.2 Experimental results

Several CNTs were evaluated for their effect on burning rate and rate exponent. It is well known that carbon powder particle size greatly influences propellant burning rate and rate exponent. The most commonly used carbon powder has an average particle size of 70 nanometers. Carbon powders of even smaller average particle size are being evaluated for future propellant applications. The results from the evaluation of the multi-walled CNTs are outlined in Table 1. The multi-walled CNTs (B, C, D, and E) all reduced propellant burning rate and significantly increased burning rate exponent to unacceptable levels. Multi-walled CNTs with either the –OH or –COOH functional group (F, G) also lowered burning rate, but the burning rate exponent was comparable to the baseline formulation containing the 70nm carbon powder. From these results, the multi-walled CNTs with either the –OH or –COOH group is considered to be more promising for possible further evaluations.

Table 1. Burning rate properties of MWCNT

CNT	Rate (in./sec.) 1000 psi	Rate (in./sec.) 1500 psi	Rate (in./sec.) 2000 psi	Rate exponent
A. Baseline: 70 nm carbon powder	0.40	0.49	0.55	0.45
B. CNT 30-50nm dia, 0.5-2μ	0.32	0.39	0.51	0.7
C. CNT, 10-20 nm dia, 0.5-2μ	0.30	0.40	0.54	0.85
D. CNT 10-20 nm dia/10-30μ	0.33	0.42	0.57	0.80
E. CNT 8 nm dia, 10-30μ	0.35	0.42	0.54	0.65
F. -COOH 95% mwnt, 50-80 nm dia/10-20μ	0.34	0.41	0.46	0.43
G. -OH 90% mwnt, 8-15 mm dia	0.30	0.37	0.43	0.50

The second group of CNTs evaluated was the single-walled with –OH or –COOH functional group. The single-walled CNTs were expected to give comparable results to the carbon powders with the additional mechanical property enhancement provided by the functional groups. The burning rate data of the single-walled CNTs are outlined in Table 2. The propellant burning rate at the 0.7% (B, D) level was slightly reduced from the baseline, but the burning rate pressure exponent was less than the baseline. A reduced rate exponent is always desirable for tactical missile applications; however, at the 1% level (C, E), the propellant burning rate was the same as the baseline with a further significant reduction of the burning rate exponent. These results indicate that both categories of CNTs could be potential candidates as replacements for carbon in future propellant applications. The lower burning rate exponents with the CNTs are very encouraging. The results here are from a small 300 gram propellant mixes; scale-up to larger mixes may yield different results.

Table 2. Burning rate properties of Single-walled (swnt) CNT with –OH and –COOH functionality.

Carbon nano-tube, CNT	Rate (in./sec.) 1000 psi	Rate (in./sec.) 1500 psi	Rate (in./sec.) 2000 psi	Rate Exponent
A. Baseline, 70 nm carbon powder	0.42	0.53	0.61	0.43
B. -OH Swnt 60%, 1-2μ, od @0.7%	0.35	0.45	0.49	0.35
C. -OH Swnt 60%, 1-2μ, od @1.0%	0.41	0.46	0.51	0.30
D. -COOH Swnt 60%, 1-2μ, od @0.7%	0.35	0.45	0.49	0.35
E. -COOH Swnt 60%, 1-2μ, od @1.0%	0.40	0.47	0.52	0.40

In addition to enhancing propellant burning rate properties, CNTs with the –OH or –COOH functional groups were expected to enhance propellant mechanical properties. The preliminary results are outlined in Table 3. Both the propellant stress and strain properties were improved, but the propellant modulus property did not show any improvements. Additional experiments, with various mixes, are needed to make a determination on the ability of CNTs

with the -OH or -COOH functional groups to improve propellant mechanical properties. One theory is that both the -OH and -COOH compete for the curing agent of the formulation which influences the overall propellant properties, especially the propellant modulus. Future efforts include a thorough investigation of how the CNTs change the cure ratio of the formulation. Small changes to the formulation are common when new ingredients are added and during each major scale-up. Lastly, methods to determine if the small improvements to mechanical property values can be further increased are evaluated.

Table 3. Initial comparison of mechanical properties of CNTs in propellant with the baseline.

Carbon nano-tube, CNT	Stress, psi	Strain,%	Modulus,psi
Baseline, 70 nm carbon powder	141	44	132
OH Swnt 60%, 1-2 μ , od @0.7%	161	74	140
OH Swnt 60%, 1-2 μ , od @1.0%	170	77	147
COOH Swnt 60%, 1-2 μ , od @0.7%	204	80	156
COOH Swnt 60%, 1-2 μ , od @1.0%	156	66	157

3.3 Technical Challenges

From these very preliminary results, both the -OH or -COOH functional single-walled CNTs may be candidates to replace carbon powder in double-base propellant formulations. There is no significant drop in propellant burning rate when either is used but the rate exponent is further reduced. Propellant rate exponents, approaching a “plateau,” are very desirable for double-base propellants.²¹ Further evaluations would have to be done with scale-up to larger mixes to exploit this property of -OH and -COOH functional CNTs. The biggest challenge to overcome for considering CNTs for propellant applications is the cost. The cost of CNTs is several times the cost of carbon powders. However, the cost of CNTs should decrease with the production of larger quantities.

4. NANO-COMPOSITES

The fourth thrust area is the development of nano-composite structures to provide enhanced vibratory protection of the weaponry’s Inertial Measurement Unit (IMU). The IMU is the key component for guidance and navigation systems aboard airborne weapons. In order to accomplish this vibratory protection effort, the AMRDEC researchers are developing advanced composite materials that provide high frequency damping for the IMU’s packaging.

The AMRDEC team, in collaboration with Materials Sciences Corporation (MSC), is developing and validating analytical models to characterize the high frequency vibration response of nanocomposite materials. Nano-filler loaded material is characterized via dynamic mechanical analysis (DMA) and vibration testing of material specimens fabricated by MSC/AMRDEC. The target application for this technology is mounting structures for instrumentation that is subject to interference from high frequency (3KHz to 20KHz) mechanical vibration during required operational environments.

4.1 Design approach

Two material configurations were identified as desirable for construction of the instrument mount: 1) IM7/8552 uni-directional prepreg, and 2) IM7/PSS compression modeled thermoplastic.

The IM7/8852 utilizes conventional hand layup fabrication methodologies, unlike the more advance IM7/PPS approach (which requires techniques such as fiber placement or compression molding). Nanotubes are sprayed between layers of the IM7/8852 prepreg during the layup process. Other programs have demonstrated the successful even dispersion of the nanotubes. A similar approach is currently underway for the compression molded IM7/PSS component. This process has not been previously demonstrated; therefore, both approaches (to achieve even distribution of the nanotubes in the compression molding process) are being evaluated.

Material testing under this program is being conducted in two stages to evaluate matrix-level effect (doped polymer) and laminate-level effect (doped polymer with continuous carbon fiber reinforcement):

Matrix level

Testing of three replicates each of nanotube doped and non-doped 8552 epoxy and PPS thermoplastic will be conducted to determine if nanotubes provide high frequency vibration attenuation. During this level of the study, dynamic mechanical analysis (DMA) and coupon level beam testing will be conducted. The DMA testing requires the materials to behave as thermo-rheologically simple materials; validating the application of the time-temperature superposition (TTS) principle.²² This allows a correspondence between tests over a low frequency bandwidth and temperature range to be used to develop the high frequency response of the material. Coupon level testing is being conducted using a mechanical shaker over the entire desired frequency bandwidth (20 kHz) to compare with the TTS assumption. The coupon level testing is being coupled with an analytical solution based on higher order plate theory. This approach assumes a displacement field that results in a parabolic through thickness shear distribution in the specimen. The shear is zero on the free surfaces of the specimen. The analytical model is more preferred than the finite element (FE)-based approach because (at higher order modes of vibration) the FE-based approach requires meshes that become computationally impractical. At high frequencies, mode interaction is common and distinction of a single mode of vibration (to relate a modal damping ratio to the material damping factor) is a technically difficult task. Coupling experimental analysis with analytical models will add a measure of justification to bandwidth averaging techniques that will require understanding of the complex modal behavior of the structure at high frequency. Experimental analysis with analytical models will add a measure of justification to bandwidth averaging techniques that will require understanding of the complex modal behavior of the structure at high frequency.

Laminate Level

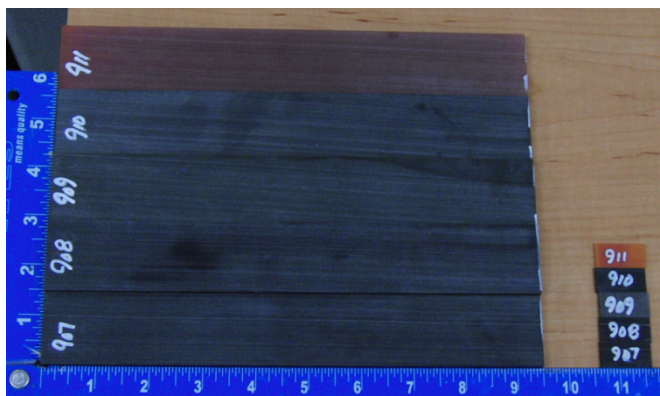
Based on the results of the matrix level testing, DMA and coupon testing (of doped and non-doped IM7/8552 laminates and IM7/PPS specimens) is being conducted. The testing is contingent on two factors:

- Does the addition of nanotubes provide increased high frequency damping for the doped matrix samples?
- Do the DMA TTS results agreed with the coupon tests?

The first factor determines which materials are carried forward as feasible material systems, and the second factor determines if the DMA TTS method is valid. If the DMA TTS method is demonstrated for these material systems, the time and effort required to generate test data are greatly reduced.

5.2 Experimental results

Initial trials were performed using nanotube doped epoxy to determine the effect at the matrix level and the applicability of the DMA TTS method.²³ These coupons were fabricated at Rensselaer Polytechnic Institute (RPI) and are pictured below (figure 14). Beam samples for classic modal analysis and DMA samples were provided to MSC.



Panel ID	Vendor ID
911	RPI_EPOXY_01
910	RPI_0.4%_MWNT_02
909	RPI_0.2%_SWNT_01
908	RPI_0.4%_SWNT_01
907	RPI_0.2%_MWNT_01

Figure 14. Carbon nanotube doped epoxy specimens from RPI

Shear modulus and loss factor data were collected on the Rensselaer Polytechnic DMA samples from 0.3 to 10 Hz over the temperature range of -50°C to 50°C in increments of 5°C. These data sets were then shifted in the frequency domain using the Williams, Landel and Ferry (WLF) equation. The Havriliak-Negami (HN) equation, which describes the complex shear modulus as a function frequency, is then fit to the shifted data. The analytical equation results in values of the shear modulus and loss factor of the material at a given temperature across the entire frequency domain.

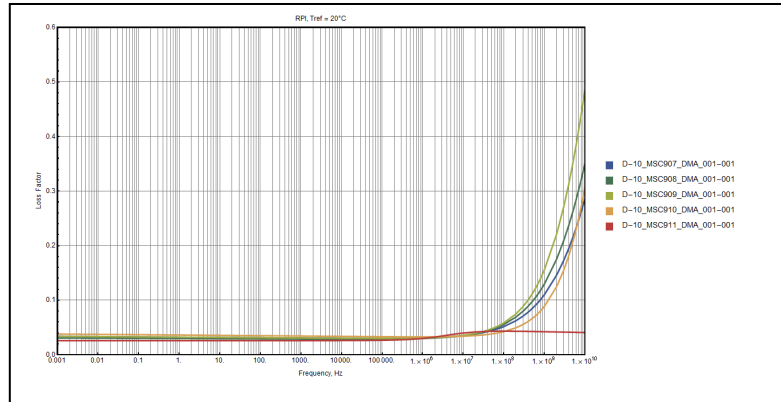


Figure 15. RPI samples loss factor as a function of frequency

Figure 15 shows the Rensselaer Polytechnic samples loss factor as a function of frequency (as a result of a TTS analysis of the experimental DMA data). All of the samples doped with nanotubes exhibited increased damping at high frequency with respect to the un-doped sample; however, it is not in the bandwidth of interest. These material systems do not result in DMA data sets that are typical of the TTS application (making use of the WLF and HN equations). Future work will be done in order to determine if other functional forms are more appropriate for TTS analysis of this material system; additionally high frequency modal analysis is still required to support these findings.

4.3 Technical challenges

The technical challenges associated with developing and validating analytical models to characterize the high frequency vibration response of nanocomposite materials are numerous. Various analytical models based on classical micromechanics are extended via linear viscoelastic theory to evaluate frequency dependent damping. Understanding of the nanotube and matrix properties and spatial distribution of the nanotubes is of primary importance to the application of these models. Since it is currently not possible to develop this data for nanotubes, test data from doped and un-doped samples is used to infer this information. Application of this modeling process is not difficult; generation of the analysis samples and accurate test data to date has been exigent.

Dispersion of nanotubes in the material systems during fabrication has been technically challenging, a limitations on matrix viscosity during processing has governed the practical limits of nanotube concentration. Additionally, uniformity of dispersion and repeatability are also issues associated with nanotube doped material systems.

The most challenging aspect of this effort is the generation of test data for the material system in the bandwidth of interest. Classical modal dynamics methods of beams are troubled by system resonances and mixed modes, making determination of damping properties at a specific frequency difficult. Both the DMA data and TTS analysis offer a possible solution to the problems associated with modal testing; however, the method is unproven and may require significant research to determine the appropriate functional forms for proper application of the TTS. The combination of a high frequency modal shaker and the analytical dynamical system models (used by the DMA to compute complex modulus data) may provide a method for conducting damping investigation at high frequency. The resulting method could be used to validate TTS analysis in the bandwidth of interest.

5. NANO-PLASMONICS

The final thrust area is the implementation of enhanced chemical detector efficiency via the development of metallic nanostructures for ultraviolet surface enhanced Raman spectroscopy. Size-controlled gallium nanoparticles deposited on sapphire are explored as alternative substrates to enhance Raman spectral signatures.²⁴ Gallium (Ga) nanoparticles (NPs) are grown using a simple, molecular beam epitaxy-based fabrication protocol. The first demonstrations of enhanced Raman signals from reproducibly tunable self-assembled Ga nanoparticles were done using visible wavelength lasers. Non-optimized aggregate enhancement factors of ~ 80 were observed from the substrate with the smallest Ga nanoparticles for crystal fast violet (CFV) dye solutions down to a dilution of 10 ppm.

5.1 Design approach

The Ga NPs can be tuned into the deep ultraviolet (UV), owing to its high plasma frequency, $\omega_p = 14\text{eV}$, with demonstrated tunability over a broad spectral range from 0.75–6.5 eV – a significant advantage over the limited range achievable by both Ag and Au, especially for simultaneous UV Raman/PL spectroscopy.^{25,26,27} Moreover, substrate-supported Ga NPs exhibit no post-deposition aggregation or attendant modification of the plasmon; therefore, the plasmon resonance is stable and reproducible. The Ga SPR remains stable and protected once oxidized even after over a year of air exposure. Conversely, Ag oxidizes excessively and becomes quenched within 36 hours of air exposure.²⁸ In addition, the Ga plasmon mode's remarkable thermal stability foreshadows Ga's advantageous use for applications in thermally harsh and diverse environments.

The Raman enhancement and longevity of Ga NPs substrates were tested using the standard Raman dye crystal fast violet (CFV).²⁴ By adjusting the deposition time at a fixed beam flux, modifications were made to the mean NP diameter and, therefore, tuned the surface plasmon resonance of three Ga NPs/sapphire substrates to (i) 2.9eV, (ii) 1.96eV, or (iii) 1.58eV, respectively, as shown in the pseudo-extinction coefficient, $\langle k \rangle$, measured by *in situ* spectroscopic ellipsometry (figure 16).^{24,25,29}

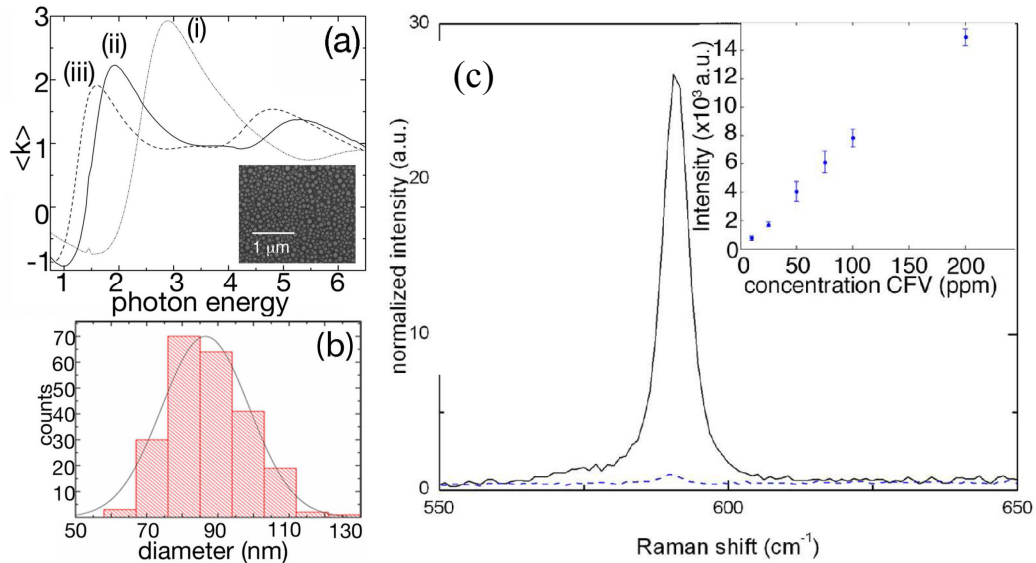


Figure 16. (a) Pseudo-extinction spectra obtained by *in situ* spectroscopic ellipsometry corresponding to three Ga NP-on-sapphire samples.²⁴ The SEM image (inset in (a)) and accompanying NP diameter distribution histogram (b) correspond to the 2.9eV SPR sample (curve (i) in (a)). A high resolution Raman spectra (c) for the strongest CFV mode at 590cm^{-1} for Ga NPs with SPR at 2.9eV (solid) compared to the same CFV mode on bare sapphire (dotted). Decreasing CFV concentration in ethanol exhibits a linear correlation between CFV concentration and the Raman intensity. Calibration error bars, determined by the standard deviation of five measurement locations, range from 4–20%, quite small even at the largest concentrations, indicating reproducibility (inset in (c)).

5.2 Experimental results

Substrates were half metallized and half unmetallized for direct comparison between the Ga NPs' influence and the bare sapphire.²⁴ The strong Raman-active CFV mode at 590cm^{-1} was measured by an inVia Raman Renishaw Raman system with a $50\times$ objective ($\sim 2\mu\text{m}$ diameter beamspot) and a 0.2mW 633nm (HeNe) laser. A 100 ppm solution of CFV in EtOH was deposited on both the metallized and bare halves of each sample. The clear difference, with and without Ga NPs on the surface, indicates that the nanostructured Ga induces an enhancement of the Raman signal [figure 16(c)]. In order to quantify the sensitivity and post-oxidation stability of enhanced Raman signal (from the 2.9eV NPs), CFV solutions (ranging from $10\text{--}200\text{ppm}$) were deposited onto Ga NPs (on sapphire) for Raman measurements [figure 16(c), inset]. As expected, the Raman intensity weakened linearly with decreasing CFV concentration; even the 10ppm sample exhibits a measurable Raman signal. In stark contrast to Ag nanostructures (that are used for SERS substrates), the Ga NP-enhanced Raman signal did not degrade even after several days of air exposure.

5.3 Technical challenges

Plasmonic Ga NPs can be flexibly applied to a variety of applications owing to their tunability over a broad spectral range, liquid phase, and attendant thermal/chemical stability. In a self-assembled, room temperature, ultra high vacuum (UHV) evaporation process, Ga NPs are tunable to specific plasmon resonances ranging from 0.75eV to 6.5eV . Although the enhancement factor for these Ga NPs is smaller than reported for Ag nanostructures, it is important to emphasize that enhanced Raman signals were observed even though room temperature deposition produces non-optimized NP density and size distributions. The tremendous control afforded by molecular beam epitaxy (MBE) deposition and Ostwald ripening to tailor Ga NP distribution (with more uniformly sized NPs or more controllable NP densities) heralds the potential of reproducibly self-assembled plasmonic Ga NPs for SERS extended into the ultraviolet.

6. SUMMARY

Collaborative efforts to transition the technologies (with both a near term impetus for commercialization of components for military systems as well as a longer term vision for less mature but innovative nanotechnology concepts) are important to the program. Currently, the Applied Nanotechnology program is developing prototypes, performing analysis, and conducting laboratory tests for the nanomaterial based sensors, composites, and propellants. The next step is to transition the technology for integration into military systems and product commercialization. The current transition plan for each functional area includes integration and relevant environment testing of the nanomaterial (sensor, composite, and/or propellant) for enhanced missile systems by 2013. By 2015, the nano enhanced missile could potentially be integrated and tested in a military environment. The integration of these critical innovative nanotechnologies into current and future weapon systems will provide enhanced understanding of missile out-gassing, increased soldier safety, reductions in missile misfires/malfunctioning of stored missiles, and decreased loads for the soldier. The rapid transition of these technologies will result in more advanced, powerful, smaller, lighter, cheaper, and safer weaponry for the warfighters.

ACKNOWLEDGEMENTS

The authors wish to express thanks to the following contractors (presented in the order the research appears in the paper) for their outstanding contributions and technical support of the AMRDEC Nanotechnology Research Initiative: 1) University of Arkansas, 2) Engenius Micro, 3) CFD Research Corporation, 4) Grace Bio Labs, 5) Miltec, Inc (Huntsville, AL), 6) ELORET (Sunnyvale, CA), 7) Materials Sciences Corporation, 8) Rensselaer Polytechnic Institute, 9) Duke University, and 10) AEGIS.

Acknowledgement is also given to DARPA for funding the SBIRs for the Nano-Enhanced Toxic Industrial Chemical Sensors. Special thanks are also given to the WDI Nano/Micro-Sensor Laboratory students (Keaira Lloyd, Tara Garrison and Akima Huggins) for assisting with the evaluation of weaponry monitoring techniques and the documentation of this paper.

REFERENCES

- [1] Ruffin, P. B., Brantley, C. L. and Edwards, E., "Innovative smart microsensors for Army weaponry applications," Proc. SPIE 6931, 6931-1 (2008).
- [2] Ruffin, P.B., Brantley, C. L. and Edwards, E., "Nano-based chemical sensor array systems for uninhabited ground and airborne vehicles," Proc. SPIE 7291, 7291-02 (2009).
- [3] Varadan, Vijay, "Development of Nanowire & SERS Based Systems For Missile & Environmental Health Monitoring and Chemical Species Detection," Final Report, DAC 0402 81249-21-0000 (2010).
- [4] Tong, Lianming, et al., *Lab Chip*, 2009, **9**, 193-195
- [5] Banerjee, Amrita, et al. *Chemical Physics Letters*, Volume 489, Issues 1-3, April 2010, pp. 121-126.
- [6] Choi, Dukhyun et al. *Lab Chip*, 2009, **9**, 239-243.
- [7] Goddard, Gregory, et al. *J. Am. Chem. Soc.*, 2010, **132** (17), pp. 6081-6090
- [8] English, Brian, "Nano-enhanced Toxic Industrial Chemical Sensors," January Report, W31P4Q-10-C-0027 (Engenius Micro) (2011).
- [9] Ketan Bhatt, Y.Wang, J. Nichols, I. Mills, K. Pant, P. Ashley, E. Webster and W. Diffey, "A Novel Nanofluidics-Based Sensor System."
- [10] R.S. Fazzio, T. Lamers, O. Buccafusca, A. Goel, and W. Dauksher, "Design and Performance of Aluminum Nitride Piezoelectric Microphones," *Transducers and Eurosensors '07, The 14th International Conference on Solid-State Sensors, Actuators and Microsystems*, Lyon, France (2007) .
- [11] S. Horowitz, D. Mathias, C. Hernandez, M. Sanghadasa, and P. Ashley, "Miniaturization of Piezoelectric Microphones," *Infotech@Aerospace Conference*, Atlanta, GA (2010).
- [12] S. Horowitz, D. Mathias, J. Cortes, M. Sanghadasa, and P. Ashley, "Miniaturized piezoelectric sensors for battlefield awareness," *National Meeting of the Military Sensing Symposia*, Las Vegas, NV (2010).
- [13] M. Royer, J. O. Holmen, M. A Wurm, O.S. Aadland, "ZnO on Si Integrated Acoustic Sensor," *Sensors and Actuators*, **4**, pp. 357-362 (1983).
- [14] S.B. Horowitz, T. Nishida, L.N. Cattafesta III, M. Sheplak, "Design and Characterization of a Micromachined Piezoelectric Microphone," *11th AIAA/CEAS Aeroacoustics Conference (26th AIAA Aeroacoustics Conference)*, Monterey, CA (2005).
- [15] E.S. Kim, J.R. Kim, R. S. Muller, "Improved IC-Compatible Piezoelectric Microphone and CMOS Process," *Solid-State Sensors and Actuators Conference (Transducers '91)*, San Francisco, CA, pp. 270-273 (1991).
- [16] R.P. Ried, E.S. Kim, D.M. Hong, R.S. Muller, "Piezoelectric Microphone with On-Chip CMOS Circuits," *Journal of Microelectromechanical Systems*, **2**, no. 3, pp. 111-120 (1993).
- [17] J. Hillenbrand, G.M. Sessler "High-sensitivity piezoelectric microphones based on stacked cellular polymer films", *Journal of the Acoustical Society of America*, **116**, no. 6, pp. 3267-3270 (2004).
- [18] S. C.Ko, Y.C. Kim, S. S. Lee, S. H. Choi, S. R. Kim, "Micromachined piezoelectric membrane acoustic device," *Sensors and Actuators A*, **103**, pp. 130-134 (2003).
- [19] L. C. Warren and J. B. Neidert, "Insensitive Minimum Signature Propellants for Joint Services Applications," JANNAF, Orlando, Florida, Dec. 6-10, (2010).
- [20] J.W. Clubb, D. G. Turnbaugh and D.W. White, "Phase II Development of Next Generation Insensitive Minimum Signature Propellants Utilizing Energetic Polymers and Novel Ingredients," JANNAF, Orlando, Florida, Dec. 6-10, (2010).
- [21] S. A. Headrick, L. Warren and S. Stiles, "Development of Lead-Free Rocket Propellant," JANNAF 2009. Hayduke, Devlin, "Nano-composite Samples," W31PQ-08-C-0189 (2010).
- [22] Christensen, R. "Theory of Viscoelasticity: Second Edition", 1982
- [23] Dlubac, J., "Polymer Test Procedures for Naval Applications", NSWCCD-72-TR—2010/103 December 2010
- [24] P.C. Wu, C.G. Khoury, T.H. Kim, Y. Yang, M. Losurdo, G.V. Bianco, T. Vo-Dinh, A.S. Brown, H.O. Everitt, *J. Am. Chem. Soc.* **131**, pp. 12032-12033 (2009).
- [25] Wu PC, Kim TH, Brown AS, Losurdo M, Bruno G, Everitt HO. "*Appl. Phys. Lett.*" **90**, pp.103119–3 (2007).
- [26] Haes AJ, Haynes CL, McFarland AD, Schatz GC, Duyne RPV, Zou S. "*MRS Bull*" **30**, pp.368–375 (2005).
- [27] Quinten M. "*Zeitschrift für Physik B Condensed Matter*" **101**, pp. 211–217 (1996).
- [28] McMahon M, Lopez R, Meyer H, Feldman L, Haglund R. "*Appl Phys B*" **80**, pp. 915–921 (2005).
- [29] Oates TWH, Mucklich A. "*Nanotechnology*" **16**, pp. 2606–2611 (2005).